The role of Sn doping in the β-type Ti–25 at%Nb alloys: Experiment and ab initio calculations

Conference Paper *in* Journal of Alloys and Compounds · May 2014

DOI: 10.1016/j.jallcom.2014.05.024

6 authors, including:

Julio Gutierrez Moreno
Barcelona Supercomputing Center
22 PUBLICATIONS **112** CITATIONS
SEE PROFILE

Yaofeng Guo
Colorado School of Mines
15 PUBLICATIONS **228** CITATIONS
SEE PROFILE

Konstantinos Georgarakis
Cranfield University
80 PUBLICATIONS **1,091** CITATIONS
SEE PROFILE

Georgos Evangelakis
University of Ioannina
130 PUBLICATIONS **1,730** CITATIONS
SEE PROFILE

Journal of Alloys and Compounds 615 (2014) S676–S679

Contents lists available at ScienceDirect

Journal of Alloys and Compounds

journal homepage: www.elsevier.com/locate/jalcom

The role of Sn doping in the β-type Ti–25 at%Nb alloys: Experiment and ab initio calculations

J.J. Gutiérrez-Moreno [a], Y. Guo [b], K. Georgarakis [b], A.R. Yavari [b], G.A. Evangelakis [c], Ch.E. Lekka [a,*]

[a] Department of Materials Science and Engineering, University of Ioannina, Ioannina 45110, Greece
[b] SIMAP-CNRS, Institut Polytechnique de Grenoble, BP 75, St. Martin d'Heres 38402, France
[c] Department of Physics, University of Ioannina, Ioannina 45110, Greece

ARTICLE INFO

Article history:
Available online 15 May 2014

Keywords:
Density functional theory
Electronic properties
XRD

ABSTRACT

β-Ti–25 at%Nb–*x*Sn alloys with several Sn substitutions ($x < 12.5$ at%) were studied by ab initio calculations and compared with the Ti–25.05 at%Nb–2.04 at%Sn rods synthesized by copper mold suction casting, annealed and water quenched. Ab initio and XRD data agree that upon Sn substitution the unit cell volume increases almost linearly. It came out that in the case of Ti–25.05 at%Nb–2.08 at%Sn, the dopant's *s*-electrons introduce low energy states (around −8 eV) with anti-bonding characteristics with the first and second neighbouring atoms, in line with the experimental findings suggesting lowering of Young modulus. At high Sn contents, first or second neighbourhood may include Sn–Sn pairs that exhibit strong direction bonds at even lower energy states, thus resulting in increase of the Young modulus. These findings, in conjunction with the calculated electronic density of states suggest that the β-phase is stable at low Sn substitutions (<6.25 at%), while higher Sn concentration ($x > 12.5$ at%) induce instability. These results could be of use in the design of ternary low rigidity biocompatible TiNbSn alloys.

1. Introduction

The β-TiNbSn ternary alloys are very promising materials for orthopaedic applications due to their biocompatibilities and their lower Young moduli [1–3] compared to Ti and TiNb systems [4–12]. Their reduced rigidity is attributed to the β-phase stabilization that is related to Nb and Sn compositions [1–3]. In particular, in the binary Ti–Nb case the β-phase becomes dominant, among the other phases, i.e. α, ω and α, basically at Nb composition higher than 25 at% [2,11], while the increase of the Young modulus in these alloys [2] is attribute to the emergence of the ω-phase, e.g. as ω particles, in the case of binary Ti–25 at%Nb [5,11,13]. The Sn presence is experimentally suggested to suppresses this ω-formation for the Ti–Nb based [2,3] alloys as well as in the Ti–Mo and Ti–V based alloys [2,14]. Specifically, in previous studies [2,3] where Sn was added to the Ti–35 wt%Nb (or Ti–21.3 at%Nb) alloy, it was found that, depending on the heat treatment, the static Young moduli of the β (Ti–35 wt%Nb)–4 wt%Sn could reach 43 GPa, while for higher Sn content, i.e. the β-(Ti–35 wt%Nb)–7.9 wt%Sn, the β-phase was more easily obtained, but the mechanical properties, even after cold rolling and several heat treatments, were not significantly improved. In addition, the Cluster–Plus–Glue–Atom model agrees with the β-phase stability of the $[SnTi_{14}]Nb_3$ ($Ti_{77.8}Sn_{5.5}Nb_{16.7}$ in at%) against the unstable $[SnTi_{14}]Nb_2$ (or $Ti_{82.3}Sn_{5.9}Nb_{11.8}$ in at%) and $[SnTi_{14}]Nb_1$ ($Ti_{87.5}Sn_{6.25}Nb_{6.25}$ in at%), which is related to the Nb (16.7 at%) and Sn (5.5 at%) compositions [15]. It turns out therefore that the presence of Sn may alter the structure and the properties of these alloys. However, the role of Sn into the Ti–Nb binary systems is not identified, while a systematic study of β-TiNbSn alloys with various Sn contents, although interesting, is still lacking. To this end, we performed linear augmented plane wave density functional theory calculations of β-Ti–25 at%Nb–*x*Sn, $x < 12.5$ at% alloys and we evaluated their structural and electronic properties for various Sn substitutions. The ab initio calculations were compared with experimental results of the Ti–25.05 at%Nb–2.04 at%Sn alloy.

2. Experimental and computational details

2.1. Experimental details

Ti–Nb binary alloys with 25.57 at%Nb and Ti–Nb–Sn ternary alloy (Ti–25.05 at%Nb–2.04 at%Sn) were synthesized in the form of large brilliant button (3–5 g) by arc-melting under Ar atmosphere from high purity Ti (99.9%), Nb (99.9%) and Sn (99.8%). The ingots were re-melted at least 6 times to ensure compositional homogeneity. The arc-melted ingots were then injected into copper molds by suction casting. The as-cast samples then underwent homogeneity treatment and were wrapped in Ti foil, encapsulated in sealed quartz tube under Ar and annealed at 1000 C for 5 h. The solution treated samples were subsequently

* Corresponding author. Tel.: +30 00302651007310.
E-mail address: chlekka@cc.uoi.gr (Ch.E. Lekka).

http://dx.doi.org/10.1016/j.jallcom.2014.05.024
0925-8388/

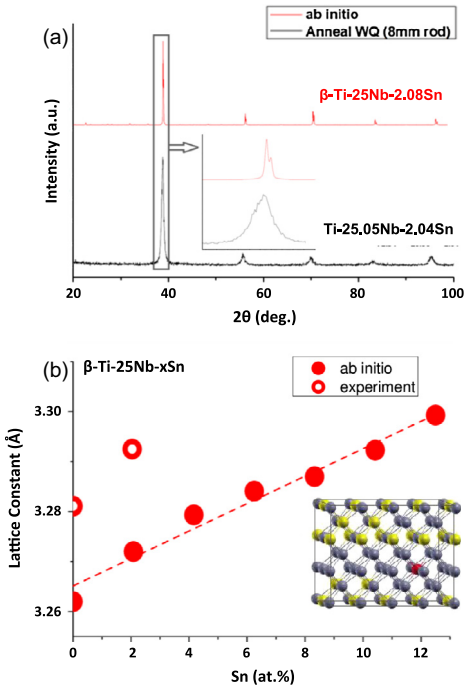

Fig. 1. (a) The conventional Cu Kα X-ray diffraction pattern of experimentally prepared Ti–25.05at%Nb–2.04 at%Sn alloy compared with the X-ray diffraction pattern of Ti–25 at%Nb–2.08 at%Sn alloy simulated with VESTA simulation package based on the β unit cell of the ab initio calculations. (b) β-Ti–25 at%Nb–*x*Sn lattice constants varying with Sn substitution. Filled and open circles correspond to ab initio and experimental data, respectively. Inset shows a schematic representation of the energetically favoured conformation of β- Ti–25 at%Nb–2.08 at%Sn. Blue and green balls stand for Ti and Sn atoms, respectively. (For interpretation of the references to color in this figure legend, the reader is referred to the web version of this article.)

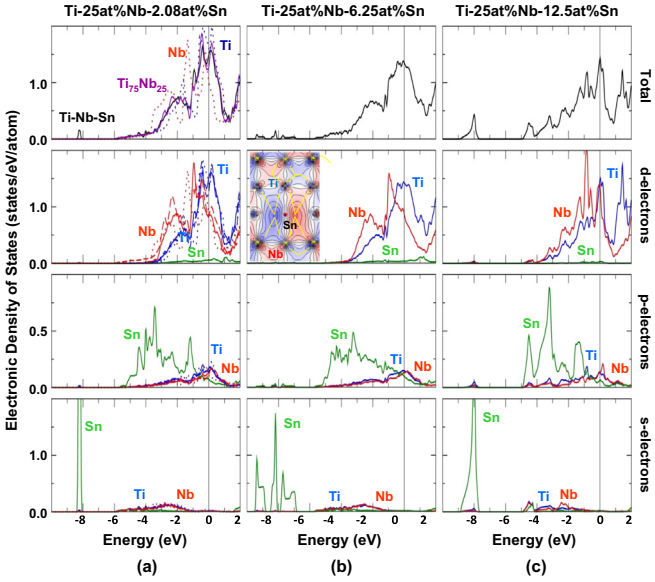

Fig. 2. Electronic density of states: (a) pure Ti, pure Nb, Ti–25 at%Nb and Ti–25 at%-2.08 at%Sn (dotted blue, dotted red, purple and black lines, respectively) for the total, *d*, *p* and *s* contributions (first up to fourth row, respectively), (b) and (c) stand for the cases of Ti–25 at%–6.25 at%Sn and Ti–25 at%–12.5 at%Sn respectively. In the inset Ti, Nb and Sn atoms are presented with grey, yellow and red balls while the red and blue values stand for negative and positive sign of the wave function (from −0.12 up to +0.12 e/Å^3). (For interpretation of the references to color in this figure legend, the reader is referred to the web version of this article.)

quenched by breaking the quartz tube in ice water. The microstructure was investigated by conventional X-ray diffraction (XRD) with Cu Kα radiation in the usual reflection mode.

2.2. Theory

Density functional theory calculations using the full-potential linearized augmented plane-wave method were applied within the WIEN2k software [16]. The generalized gradient approximation GGA was employed for the exchange correlation functional in the form given by Perdew, Burke, and Ernzerhof (PBE96) [17], while the self-consistency is assumed for a total energy convergence less than 10^{-4} Ry. Several unit cells were used to account for the various cases of Sn substitutions and sampling of the Brillouin zone. For all compositions we used 48 basis atoms along with a $6 \times 4 \times 3$ (38) k-point meshes. In line with the compositions utilized in the experiments, we kept constant Nb concentration at 25 (at%), while Ti was progressively substituted by Sn in concentrations starting from Ti–25 at%Nb–2.0 8at%Sn (corresponding to 1 Sn atom per 48 supercell atoms) up to Ti–25 at%Nb–12.5 at%Sn (6 Sn atoms per supercell). We note that this approach, although not the same, is the closest to the experimental situation. We used several different atomic configurations, in which the distributions of the Nb atoms and their short range Sn neighborhood were systematically tested. From all atomic configurations, the energetically favored were chosen for further studies which were mainly related with the presence of Sn–Ti first neighbor atoms (e.g. total energy curves, equilibrium lattice constant, bulk moduli and electronic density of states). The initial structures were treated under hydrostatic pressure and the total energy versus volume of the primitive unit cell curve was fitted by the Birch–Murnaghan equation of state determining the optimum lattice parameters and the bulk moduli. The powder diffraction pattern simulations were performed within the VESTA software [18] taking as input the energetically favored unit cell calculated by the WIEN2k code.

3. Results and discussion

3.1. Structural properties

Fig. 1a depicts the X-ray diffraction patterns of Ti–25.05 at%Nb–2.04 at%Sn together with the simulated VESTA β-Ti–25 at%Nb–2.08 at%Sn powder diffraction pattern using the ab initio unit cell. From the experimental XRD, only peaks corresponding to the β phase are identified, while no sign of the ω-phase is observed. In line with the bulk Ti-based alloys, the highest intensity first peak corresponds to the (1 1 0) preferred orientation. This peak refers to the first textured preferred growth direction. It is interesting to notice that despite the limitations of the single phase monocrystalline matrix of the ab initio calculations, as well as the "powder" approximation of the VESTA software, there is an overall agreement between the experimental and the theoretical XRD diffraction data. In particular, in the inset of Fig. 1a, although the first XRD experimental peak is wider than the theoretical one, the corresponding angles of the main peak are almost the same. Finally, both theoretical and experimental relative distances between the XRD peaks are comparable.

In Fig. 1b, we provide the lattice constants obtained from the ab initio computations (filled circles) juxtaposed with the available experimental data from the XRD measurements (open circles). Interestingly, although the theoretical values are lower from the experimental ones, they both exhibit the same slope. This is attributed to the fact that the calculations refer to single crystal at zero temperature, while experimentally the alloys are polycrystalline and are measured at room temperature.

One of the ab initio total energy calculations outcomes is the bulk modulus (B). We found that upon Sn substitutions the B values are slightly increasing from 119 GPa (Ti–25 at%Nb–2.08 at%Sn) to 127 GPa for Ti–25 at%Nb–12.5 at%Sn.

3.2. Electronic properties

Aiming in obtaining insight on the role of Sn and in order to reveal the electronic origin (if any) of both β-phase stability and alterations of the mechanical properties, we evaluated the Electronic Density of States (EDOS) of pure Ti and Nb, binary alloy, as

well as ternaries for selective compositions, i.e. for the β-Ti–25 at%Nb–*x*Sn, *x* = 2.08, 6.25 and 12.5, Fig. 2.

Starting with the pure Ti EDOS, we observe two main energy bands located around −2 eV and at the Fermi level (E_F) separated by a minimum at −1 eV. Close to E_F a local minimum at + 0.1 eV is found between the highest occupied state (around −0.5 eV) and the first unoccupied one (at 0.25 eV) that persists in the binary Ti–25 at%Nb and ternary Ti–25 at%Nb–2.08 at%Sn cases. The pure Nb EDOS exhibits a low energy band around −2.5 eV, while the next one is located far from E_F, denoting higher stability of the Nb β-phase compared to the previous cases. The presence of Sn introduces a low energy state at −8.2 eV, while slight depletion is found at the Fermi level without altering significantly the characteristics of the binary β-phase's EDOS. In the Ti–25 at%Nb–6.25 at%Sn total EDOS, the energy states are depleted at E_F, causing an almost equivalent occupancy from –1 eV up to 1 eV, while no difference is found between the three Sn compositions at the lower energy states close to −8 eV. On the contrary, in the case of the highest Sn content (Ti–25 at%Nb–12.5 at%Sn) the EDOS exhibits a peak at E_F and a general reduced occupancy in the occupied states, denoting instability of the β-phase for this composition [19] in line with the Cluster–Plus–Glue–Atom model [15]. It worth's to be noted that the alterations at EF are due to the relative compositional changes upon Sn substitutions and not to direct Sn contributions, i.e. more Nb content. This is nicely illustrated in the calculated partial *s*, *p* and *d* EDOSs, Fig. 2, in which we can see that the *d*-electron EDOS is due to contributions from Nb and Ti atoms. In all ternaries, Ti_{3d}–Ti_{3d}, Nb_{4d}–Nb_{4d} and Ti_{3d}–Nb_{4d} π-like bonding states are manifested as shown in the energy contour (isovalue around −3 eV), inset in Fig. 2. For the 2.08 and 6.25 at% Sn compositions, the Ti *d*-electrons are mainly responsible for the EDOS features at E_F, while for the 12.5 at% Sn case the Nb d-electron appear

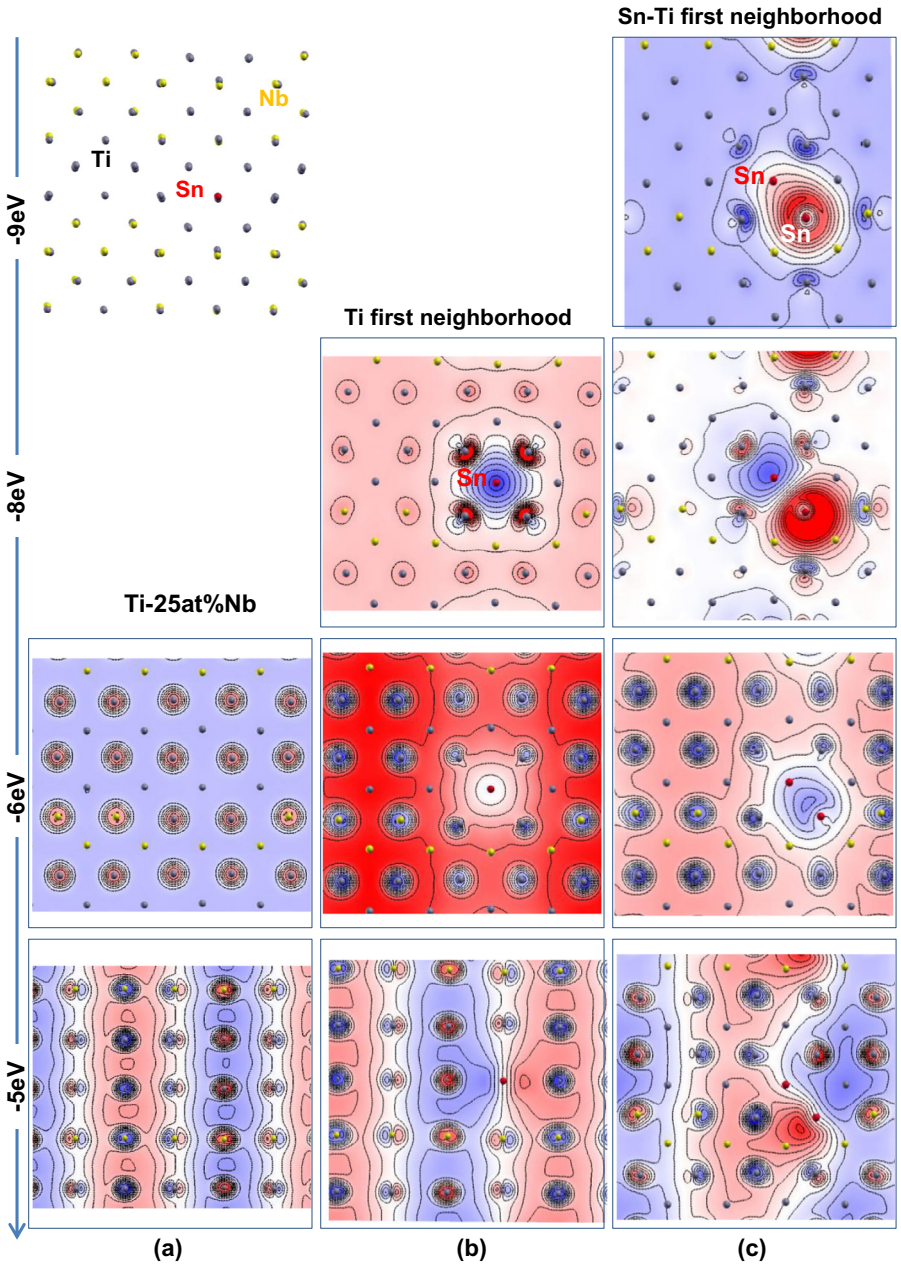

Fig. 3. The wavefunctions at selective energies at a plane containing the Sn atoms: (a) binary Ti–25 at%Nb and (b) or (c) ternary alloy with Sn atom having Ti or Ti–Sn first neighboring atoms, respectively. Ti, Nb and Sn atoms are presented with grey, yellow and red balls while the red and blue values stand for the negative and positive sign of the wave function (from −0.12 up to +0.12 e/Å^3). (For interpretation of the references to color in this figure legend, the reader is referred to the web version of this article.)

also at E_F. This is due to Nb_{4d}–Sn_{5p} hybridizations occurring when these atoms become first neighbours, i.e. at high Sn contents. The *s* and *p* partial EDOSs are dominated by Sn contributions. A broad band energy from –1 eV down to −6 eV characterizes the *p*-electron EDOS, while the states from −7 eV down to −9 eV are due to *s*-electrons.

In addition, we investigated in detail the bonding characteristics of the dopant, focusing on the energies that were appearing from the EDOSs significant for possible hybridizations. The wavefunctions at the lowest energies for the binary and the ternaries are depicted in Fig. 3a–c, respectively. The clear metallic character is visible for the former alloy in the [100] plane around −6 eV. Similar behavior is found at −5 eV in the [100] plane, while in the [010] plane the electronic hybridizations' are characterized by antibonded successive rows of s bonded electrons and p semicore Nb or Ti electrons. Upon Sn substitution these states are altered, as manifested clearly by the broken symmetry that is due to *s* Sn *p* Ti hybridization at −5 eV and *s*–*s* Sn–Ti bonding at −6 eV, Fig. 3b. The new state at −8 eV is due to *s*–*d* antibonding between Sn and Ti atoms. We should note that the energetically favoured configuration corresponds to Sn–Ti first neighboring atoms, followed by a mixed Ti–Nb neighbourhood. Thus, at high Sn contents, Sn atoms become also first neighbors, inducing significant modifications in the bonding characteristics due to *p*–*p* at −5 eV and *s*–*s* at –6 eV hybridizations, thus changing locally the electronic character. Interestingly, the antibonding state found previously at −8 eV preserves its character, while another lower bonding state at −9 eV is manifested that is due to *s*–*s* hybridizations. These findings suggest that relatively low Sn substitutions may reduce the rigidity (by means of local antibonding sites), while high Sn content results in significant deterioration of the periodic symmetry of the electronic charge that may lead to mechanical instability.

4. Conclusions

We presented experimental and computational results on the β-TiNbSn alloys. From the XRD measurements we found an almost linear increase of the lattice constants upon Sn substitutions, while although underestimated the ab initio values follow the experimental behavior. The electronic density of states reveal that the Ti–25 at%Nb–12.5 at%Sn β-phase is energetically un-favoured compared to the Ti–25 at%Nb–2.08 at%Sn and Ti–25 at%Nb–6.25 at%Sn. Sn *s*-electrons are responsible for the lowest energy states around −8 eV, the Sn *p*-electrons are located at energies below −3 eV, while Ti *d*-electrons contribute mainly at the Fermi level. In addition, it came out that at relatively low Sn substitutions results in local antibonding sites, while high Sn content leads to significant modifications of the electronic charge symmetry and may lead to mechanical instability. These results could be use for the design of β-Ti-based alloys with non-toxic additions, suitable for orthopedic applications.

Acknowledgment

This work was supported by the BioTiNet ITN (No. 264635) FP7 Marie Curie project.

References

[1] Y. Guo, K. Georgarakis, Y. Yokoyama, A.R. Yavari, J. Alloys Comp. 571 (2013) 25–30.
[2] T. Ozaki, H. Matsumoto, S. Watanabe, S. Hanada, Mater. Trans. 45 (2004) 2776–2779.
[3] H. Matsumoto, S. Watanabe, S. Hanada, Mater. Trans. 46 (2005) 1070–1078.
[4] C.M. Lee, C.P. Ju, J.H. Ju, J. Oral Rehabil. 29 (2002) 314–322.
[5] D.L. Moffat, U.R. Kattner, Metall. Trans. A 19 (1988) 2389–2397.
[6] E.W. Collings, Physical Metallurgy of Titanium Alloys, The American Society of Metals, Materials Park, OH, 1984.
[7] R. Boyer, G. Welsch, E.W. Collings, Materials Properties Handbook: Titanium Alloys, ASM International, Materials Park, OH, 1994.
[8] R. Hermann, H. Hermann, M. Calin, B. Büchner, J. Eckert, Scr. Mater. 66 (2012) 198–201.
[9] S. Banumathy, R.K. Mandal, A.K. Singh, J. Appl. Phys. 106 (2009) 093518.
[10] D. Kuroda, M. Niinomi, H. Fukui, M. Morinaga, A. Suzuki, J. Hasegawa, Tetsu Hagane 86 (2000) 602–609.
[11] H.Y. Kim, Y. Ikehara, J.I. Kim, H. Hosoda, S. Miyazaki, Acta Mater. 54 (2006) 2419–2429.
[12] A.I. Mardare, A. Savan, A. Ludwig, A.D. Wieck, A.W. Hassel, Electrochim. Acta 54 (2009) 5973–5980.
[13] Y.H. Hon, J.Y. Wang, Y.N. Pan, Mater. Trans. 44 (2003) 2384–2390.
[14] J.C. Williams, B.S. Hickman, D.H. Leslie, Metall. Mater. Trans. B 2 (1971) 477–484.
[15] Q. Wang, C. Ji, Y. Wang, J. Qiang, C. Dong, Metall. Mater. Trans. A 44 (2013) 1872–1879.
[16] P. Blaha, K. Schwarz, G.K.H. Madsen, D. Kuasnicka, J. Luitz, WIEN2K, Augmented Plane Wave Local Orbitals Program for Calculating Crystal Properties, Vienna University of Technology, Vienna, Austria, 2001.
[17] J.P. Perdew, K. Burke, M. Ernzerhof, Phys. Rev. Lett. 77 (1996) 3865–3868.
[18] K. Momma, F. Izumi, J. Appl. Crystallogr. 44 (2011) 1272–1276.
[19] P. Soederlind, O. Eriksson, J.M. Wills, A.M. Boring, Phys. Rev. B 48 (1993) 5844–5851.